Cretaceous Research 91 (2018) 20–32

Contents lists available at ScienceDirect

Cretaceous Research

journal homepage: www.elsevier.com/locate/CretRes

An integrated pelagic carbonate multi-proxy study using portable X-ray fluorescence (pXRF): Maastrichtian strata from the Bottaccione Gorge, Gubbio, Italy

Matthias Sinnesael [a, *], Niels J. de Winter [a], Christophe Snoeck [a], Alessandro Montanari [b], Philippe Claeys [a]

[a] Analytical, Environmental and Geo-Chemistry, Vrije Universiteit Brussel, Pleinlaan 2, B-1050 Brussels, Belgium
[b] Osservatorio Geologico di Coldigioco, Cda. Coldigioco 4, 62021 Apiro, Italy

ARTICLE INFO

Article history:
Received 5 December 2017
Received in revised form
18 March 2018
Accepted in revised form 11 April 2018
Available online 18 May 2018

Keywords:
Portable X-ray fluorescence (pXRF)
Pelagic carbonates
Cyclostratigraphy
Chemostratigraphy
K-Pg boundary
Maastrichtian
Gubbio

ABSTRACT

Pelagic carbonate sections constitute common archives for paleoclimatological and stratigraphical research. This study evaluates the use of portable X-ray fluorescence (pXRF) measurements on pelagic carbonates and applies the method to the well-studied latest Maastrichtian in the Bottaccione Gorge section from Gubbio, Italy. A calibration with carbonate reference materials makes it possible to acquire absolute elemental concentrations, and allows for comparison with results from previous geochemical studies, which used more expensive and time consuming conventional techniques, such as neutron activation or Inductively Coupled Plasma Mass Spectrometry (ICP-MS). With adequate measurement strategies and careful calibration, pXRF measurements can be a reliable, non-destructive, cheap, fast and easy to use alternative to acquire multi-elemental concentration data (Ca, Fe, Mn, Sr) in pelagic carbonates. These pXRF elemental concentration data represent valuable additions to classical proxies such as magnetic susceptibility and calcium carbonate content used in the study of pelagic carbonates. Furthermore, the potential of the portable pXRF method for applications in cyclostratigraphical (e.g. using Fe-concentrations) and chemostratigraphical (e.g. using Mn and Sr concentrations) investigations is demonstrated. A strong covariation between the measured Sr concentration profile obtained by pXRF and the existing $\delta^{18}O$ record, in combination with micro-XRF mapping, demonstrated the sampling of calcite veins in some of the samples. The first $^{87}Sr/^{86}Sr$ isotope measurements for the latest Maastrichtian in the Bottaccione Gorge section seem to be little affected by this sampling effect.

1. Introduction

Multiple studies have measured major, minor and trace elemental concentrations at the well-known Cretaceous-Paleogene boundary interval at the Bottaccione Gorge, Gubbio, Italy (e.g. Alvarez et al., 1980; Renard et al., 1982; Smit and Ten Kate, 1982; Calderoni and Ferrini, 1984; Lowrie et al., 1990; Sosa-Montes de Oca et al., 2017). These elemental concentrations were obtained using various analytical techniques, such as neutron activation analysis, laboratory scale X-ray fluorescence (XRF), Inductively Coupled Plasma Mass Spectrometry (ICP-MS) or Inductively Coupled Plasma Emission Spectrometry (ICP-OES). These conventional techniques are expensive and require extensive sample preparation and measurement time. Recently, Quye-Sawyer et al. (2015) and de Winter et al. (2017a) demonstrated that certain major, minor and trace elements in carbonates (e.g. Ca, Mn, Fe and Sr) can be measured accurately using a portable X-ray fluorescence spectrometer (pXRF). Ibáñez-Insa et al. (2017) showed that the pXRF could be used to pinpoint the Cretaceous-Paleogene boundary clay in the marly sections of Agost and Caravaca. The present study applies pXRF to the Bottaccione Gorge section in Gubbio, Italy, in an attempt to quickly obtain reliable major and minor element data that can then be used in chemostratigraphy or cyclostratigraphy studies.

The potential advantages of pXRF are multiple: e.g. the non-destructive nature of the technique, the possibility of *in-situ* analysis, the requirement of little to no sample preparation, the relative ease of use, and the fact that it is a less expensive and much faster

* Corresponding author.
E-mail address: Matthias.Sinnesael@vub.be (M. Sinnesael).

https://doi.org/10.1016/j.cretres.2018.04.010
0195-6671/

alternative to more conventional devices such as ICP-MS. However, the pXRF method typically has higher limits of detection for most elements, lower accuracy and lower precision compared to more conventional XRF or ICP-MS applications (e.g. Young et al., 2016; Thibault et al., 2017; de Winter et al., 2017a). Also, for *in-situ* pXRF measurements (e.g. on geological sections), the role of specific aspects such as outcrop weathering and surface effects needs to be taken into consideration (e.g. Potts et al., 2006; Quye-Sawyer et al., 2015).

The goal of this study is to investigate how, and for which elements, the pXRF can be used reliably to collect high-resolution reproducible elemental concentration records from a stratigraphic interval of pelagic carbonates. In the field, pXRF measurements carried out directly on the surface of the selected interval of the Bottaccione Gorge gave non-reproducible results – mainly because of the weathered and rough topography of the outcrop, preventing a solid and steady contact between pXRF nozzle and the measured sediment. Therefore, we moved to the laboratory and use the pXRF to measure powdered samples collected and described by Sinnesael et al. (2016a). To calibrate these pXRF measurements, seven certified carbonate reference materials are used. The calibrated elemental concentrations measured by pXRF are compared with results from other studies, which use a range of conventional analytical techniques for measuring trace element concentrations (Renard et al., 1982; Smit and Ten Kate, 1982; Sosa-Montes de Oca et al., 2017). Besides these elemental concentration data, there is an abundance of other available geochemical and sedimentological proxy data for this well-studied interval: magnetic susceptibility, calcium carbonate content, Helium (^{4}He and ^{3}He) isotopes, Osmium (^{187}Os/^{188}Os) isotopes, bulk oxygen (δ^{18}O) and carbon (δ^{13}C) stable isotopes (e.g. Corfield et al., 1991; Mukhopadhyay, 2001; Robinson et al., 2009; Voigt et al., 2012; Husson et al., 2014; Sinnesael et al., 2016a). This wealth of data produces a detailed integrated multi-proxy study where the relationship between various proxies can be investigated. As such, we compare the well-established magnetic susceptibility and calcium carbonate content proxies with the Fe and Ca concentrations obtained by pXRF. Furthermore, we evaluate the robustness of pXRF data for cyclostratigraphical analysis by comparing results in this study with those of the numerous cyclostratigraphical studies that have been carried out in the Umbria-Marche basin sections (e.g. Herbert et al., 1986; Cleaveland et al., 2002; Husson et al., 2012; Husson et al., 2014; Galeotti et al., 2015; Batenburg et al., 2016; Sinnesael et al., 2016a,b; Giorgioni et al., 2017; Montanari et al., 2017). As proxies for cyclostratigraphical analyses we use proxies which reflect the (climate sensitive) transport of clasts and particles from the continent towards the basin (detrital input). Examples of such proxies are: magnetic susceptibility and elements such as Potassium (K), Titanium (Ti) and Iron (Fe) versus the biogenic input or $CaCO_3$ content Additionally, we explore the potential of pXRF to carry out chemostratigraphy on pelagic carbonates; this in combination with looking at existing δ^{13}C data and presenting the first ^{87}Sr/^{86}Sr results for the classic terminal Maastrichtian in Gubbio.

2. Geological and stratigraphic setting

The classical sections of Gubbio (Fig. 1, Umbria region, Italy) are well-known from a variety of studies, in particular the Bottaccione

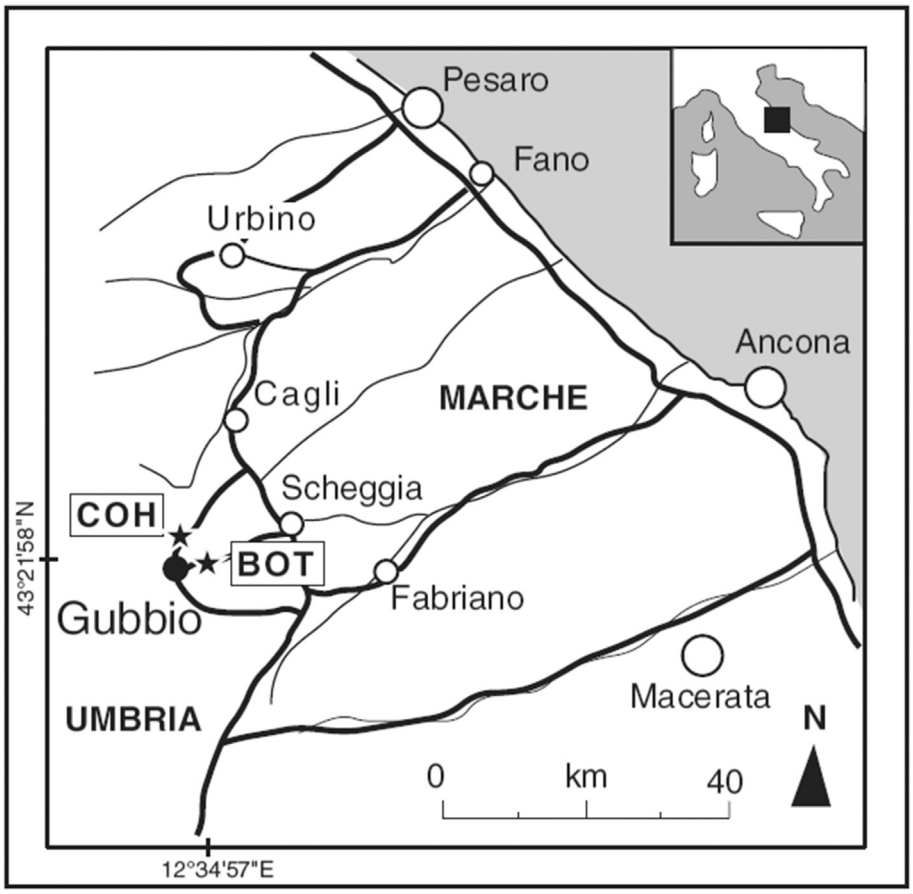

Fig. 1. Geographical location of the stratigraphic sections near the town of Gubbio, Italy (43°21′58″ N, 12°34′57″ E). BOT = Bottaccione Gorge section; COH = Contessa Highway section.

Gorge where the K-Pg boundary was biostratigraphically defined for the first time by Luterbacher and Premoli Silva (1964). It is also in the Bottaccione Gorge section that Alvarez et al. (1980) first reported the iridium anomaly that led to the hypothesis of an asteroid impact causing the K-Pg boundary mass extinction.

The section of the Bottaccione Gorge (BOT) investigated in this work is part of the continuous Umbria-Marche Basin succession of pelagic carbonates spanning the early Jurassic to the late Miocene. It is located in the R2 member of the Scaglia Rossa Formation (Montanari et al., 1989), which is characterized by pink biomicritic limestone made up of planktonic foraminiferal tests suspended in a coccolith matrix with a terrigenous component of silt and clay considered to be of eolian origin (Arthur and Fischer, 1977; Johnsson and Reynols, 1986; Savain et al., 2014; Sinnesael et al., 2016a). The reported biostratigraphy is from Coccioni and Premoli Silva (2015) which for this specific interval largely agrees with the biostratigraphy of Gardin et al. (2012), and the magnetostratigraphy from Lowrie et al. (1982) (Fig. 2). This study deals with the same stratigraphic interval (7.2 continuous meters of section below the K-Pg boundary, sampled every 5 cm) discussed in detail (integrated bio-, magneto-, chemo- and cyclostratigraphy) by Sinnesael et al. (2016a, and references therein).

3. Materials and methods

Sinnesael et al. (2016a) collected a total of 145 powdered samples from the upper 7.2 m of the Maastrichtian in the BOT section, sampled at regular 5 cm intervals using an electric drill. These same samples are measured at the Vrije Universiteit Brussel (hereafter: VUB, Brussels, Belgium) using a Bruker Tracer IV Hand Held portable XRF device (HHpXRF, hereafter: pXRF) equipped with a 2 W Rh anode X-ray tube and a 10 mm^2 Silicon Drift Detector (SDD) with a resolution of 145 eV (Mn-Ka). The X-ray beam is focused on a 6 mm by 8 mm integrated area, using a Pd collimator. X-ray spectra from the pXRF are deconvoluted and quantified using the standard factory "*Soil Fundamental Parameters*" method. The fundamental parameters method makes use of the theoretical relationship between X-ray fluorescence and material composition as determined by Sherman (1955). The factory-calibrated quantification method of the pXRF uses this fundamental principle with a correction based on the matrix effect observed in soil and rock samples. All pXRF measurements are carried out by putting the pXRF nozzle directly (without films) on the powder surface. All analyses are duplicated with a measurement time of 30 s and concentrations reported in this study are averages of two measurements.

The pXRF results are calibrated using the following set of 7 certified carbonate powder standards: CCH-1 (Liège University), COQ-1 (United States Geological Survey, USGS), CRM393 (Bureau of Analysed Samples, BAS), CRM512 (BAS), CRM513 (BAS), ECRM-782-1 (BAS) and SRM-1d (National Institute of Standards and Technology, NIST). The carbonate standard powders were loaded in open plastic sample containers and measured in the same way as the BOT samples. The results of pXRF measurements on the carbonate reference materials as well as certified values and their documented errors are given in Supplementary Materials ("Tab. S1 Carbonate Reference Materials"). Besides their potential as paleoenvironmental proxy, the selection of elements Potassium (K), Calcium (Ca), Titanium (Ti), Manganese (Mn), Iron (Fe), Strontium (Sr) is based on the available certified values of used reference materials for calibration and the specific pXRF set-up in this study, which does not allow for the reliable detection of light elements, like Magnesium (Mg), Aluminum (Al) and Silicon (Si). Since both certified concentrations of standards and concentrations measured by pXRF possess a known error, a Deming regression is applied using the "*Deming*" protocol available in the open source computational software package R (R Development Core Team, 2008) to establish the calibration curve. The complete R-script used to execute the Deming regression for every calibration is also given in Supplementary Materials ("R-script Deming regression XRF"). The Deming regression incorporates uncertainties on both the dependent and the independent variable in the calculation of the linear regression curve, as opposed to more commonly used simple linear regression model, which only considers uncertainties on the dependent variable (Adcock, 1878; Kummell, 1879; Deming, 1943; Thiel, 1950). Based on Deming regression, calibration curves are established for concentrations of K, Ca, Ti, Mn, Fe and Sr measured by pXRF. Table 1 lists the resulting slopes and intercepts values of the calibration curves for every element including their errors (1 σ) and Pearson's coefficients of the regressions. Deming regression curves of a selection of elements (Ca, Mn, Fe and Sr) are shown in Fig. 3. The calibrated elemental concentrations of the pXRF measurements carried out for K, Ca, Ti, Mn, Fe and Sr are available in the Supplementary Materials ("Tab. S2 Results pXRF Calibrated Sr Isotopes and $\delta^{13}C$ and $\delta^{18}O$ carbonate isotopes").

Micro-XRF measurements were carried out at the VUB using the Bruker M4 Tornado micro XRF (hereafter: μXRF) under vacuum conditions (20 mbar). The μXRF is equipped with a 30 W Rh anode metal-ceramic X-ray tube and two 30 mm^2 Silicon Drift Detectors with a resolution of 145 eV (Mn-Ka). The X-ray beam was focused by using poly-capillary lens on a spot with a diameter of 25 mm (Mo-Ka). Micro-XRF line scanning was done according to the point-by-point scanning method outlined in de Winter et al. (2017b), using an integration time of 60 s. This integration time was sufficient for Time of Stable Reproducibility (TSR) and Time of Stable Accuracy (TSA) to be reached for individual point spectra for all elements considered in this study (see de Winter et al., 2017a). X-ray spectra were deconvoluted and quantified with Bruker Esprit software using FP quantification relative to the CRM393 limestone standard. Results for individual points on the line scans were calibrated using the same range of carbonate reference materials used for calibration of the pXRF results in this study. Micro-XRF mapping was carried out on the Bruker M4 in mapping mode using short integration time (1 ms) per pixel. These conditions allowed concentrations of major and trace elements to be characterized only semi-quantitatively (see de Winter et al., 2017b). The sample measured with μ-XRF was a polished hand sample taken around level −1.50 m in the BOT section, which contained a clear calcite vein (Fig. 6).

Stable isotope measurements of the bulk carbonate rock for $\delta^{13}C$ (‰ Vienna Pee Dee Belemnite, VPDB) and $\delta^{18}O$ (‰ VPDB) were also carried out at the VUB using a Nu Perspective isotope ratio mass spectrometer (IRMS, Nu Instruments, UK) interfaced with a Nu Carb automated carbonate device. Acidification of the samples occurred at a temperature of 70 °C. Calibration was carried out using an in-house Carrara marble (MAR2_2) standard (+3.41‰ VPDB, −0.13‰ VPDB), which is calibrated against NBS-19. On the basis of replicated measurements of the MAR2_2 standard, the error on the $\delta^{13}C$ and $\delta^{18}O$ was estimated as <0.05‰ (1 σ) and <0.10‰ (1 σ), respectively. Three different types of sample were drilled from the acquired hand sample around level −1.50 m and are their locations are indicated on Fig. 6. One sample contained pure calcite from a calcite vein, another sample contained a pure pink micritic matrix and one more sample contained a mix of a calcite vein and matrix material. Every sample was measured in duplicate. The corrected $\delta^{13}C$ and $\delta^{18}O$ carbonate isotope values are available in the Supplementary Materials ("Tab. S2 Results pXRF Calibrated Sr Isotopes and $\delta^{13}C$ and $\delta^{18}O$ carbonate isotopes").

The Sr isotopes ($^{87}Sr/^{86}Sr$) of 12 samples taken at ± 50 cm intervals from the terminal Maastrichtian in the Bottaccione Gorge were measured by Multi-Collector Inductively Coupled Plasma

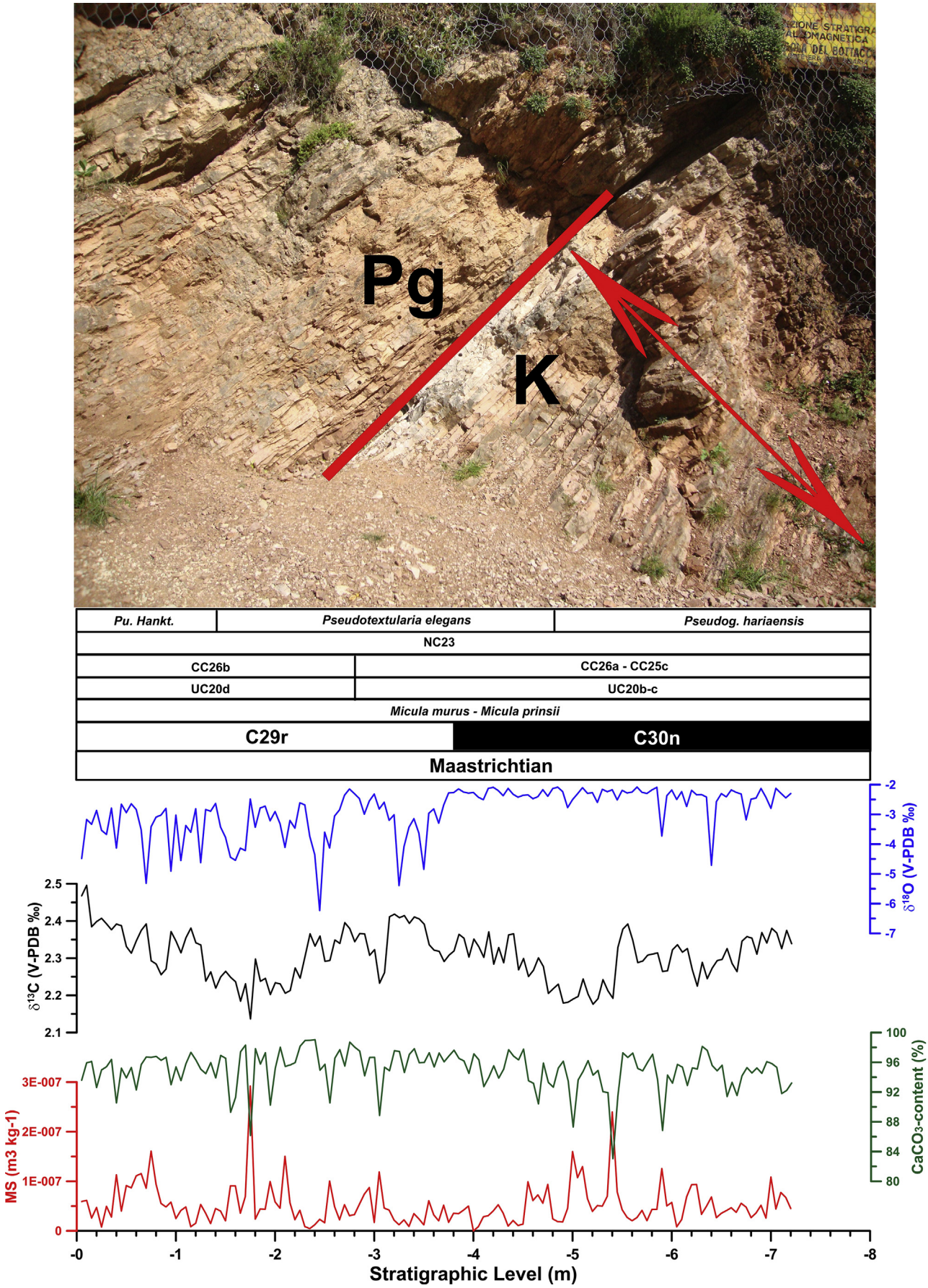

Fig. 2. Detail of the Bottaccione section (BOT), with the reported magnetic susceptibility (MS), calcium carbonate content ($CaCO_3$), and bulk $\delta^{18}O$ & $\delta^{13}C$ from Sinnesael et al. (2016a). The same upper Maastrichtian powdered samples are analyzed with the pXRF in this study (7.2 continuous meters of section below the K-Pg boundary, sampled every 5 cm).

Table 1
Deming regression parameters for the pXRF calibration curves.

Deming regression parameters					
Element	Slope	Error on slope	Intercept (ppm)	Error on intercept (ppm)	Pearson's r
K	0.17	9.04	−452	68114	0.5417
Ca	0.4	0.03	116320	16087	0.9947
Ti	4.07	1.01	−13	26	0.9461
Mn	0.66	0.02	34	9	0.9999
Fe	0.61	0.05	−45	71	0.9995
Sr	0.94	0.07	33	9	1

Mass Spectrometry (MC-ICP-MS) at the GTime laboratory of the Université Libre de Bruxelles, Belgium (hereafter ULB). To extract the Sr present in the carbonate fraction of the samples and avoid the Sr from the silicate and other fractions, about 50 mg of powdered sample were placed in Savillex® reaction tubes together with 2 mL of 1 M HCl at room temperature and left to react for 24 h. The supernatant was recovered and centrifuged to eliminate any non-carbonate residue. The supernatant is then evaporated on a hotplate at 105 °C for 12 h. The entire acid digestion process and subsequent Sr purification were achieved under a class 100 laminar flow hood in a class 1000 clean room atULB. The dried residues were digested in subboiled concentrated 14 M HNO_3 at 120 °C for 2 h, before purification of the Sr analyte by a chromatographic technique using ion-exchange resins, as detailed in Snoeck et al. (2015). The isotope ratios of the purified strontium samples are then measured on a Nu Plasma MC-ICP mass spectrometer (Nu Instruments Ltd, Wrexham, UK) at ULB. During the course of this study, repeated measurements of the NBS987 standard solution yielded a value of $^{87}Sr/^{86}Sr = 0.710214 \pm 40$ (2 σ for 15 analyses), which is consistent with an average of 0.710252 ± 13 (n = 88; 2 σ) obtained by Thermal Ionization Mass Spectrometry (TIMS, Weis et al., 2006) on the same standard. All the data are corrected for mass fractionation by internal normalization to a $^{86}Sr/^{88}Sr$ ratio of 0.1194. In addition, after the measurements all the raw data are normalized using a standard-sample bracketing method with the recommended value of $^{87}Sr/^{86}Sr = 0.710248$ for NBS987 (Weis et al., 2006). For each sample the $^{87}Sr/^{86}Sr$ value is reported with a 2 σ error (absolute error value of the individual sample analysis – internal error). The corrected Sr isotope values are available in the Supplementary Materials ("Tab. S2 Results pXRF Calibrated Sr Isotopes and $\delta^{13}C$ and $\delta^{18}O$ carbonate isotopes").

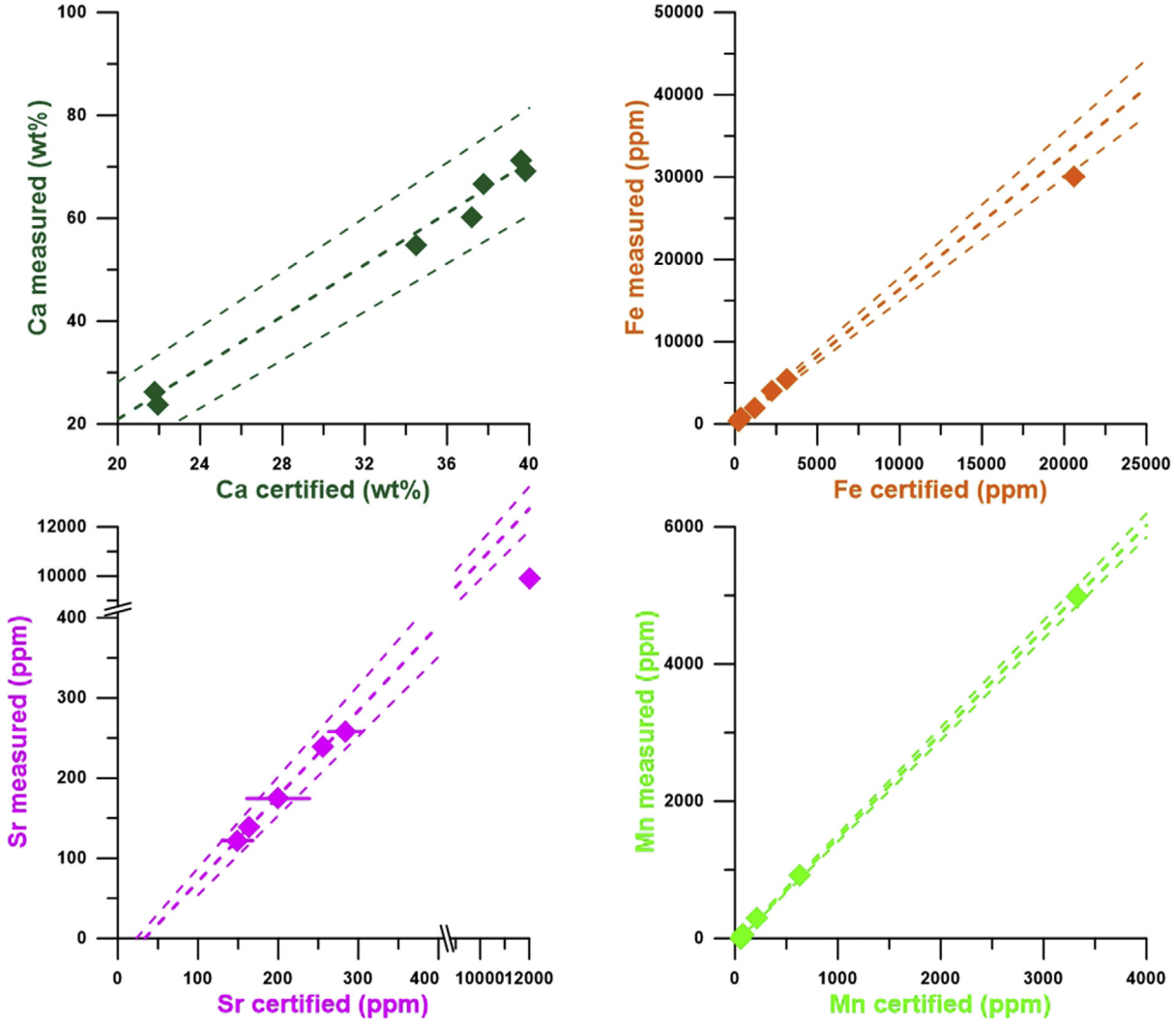

Fig. 3. Calibration curves for pXRF measurements from the 7 certified carbonate powder standards (CCH-1, COQ-1, CRM393, CRM512, CRM513, ECRM-782-1 and SRM-1d) for Ca (dark green), Fe (orange), Sr (magenta) and Mn (light green). Error bars (1 σ) for both certified and pXRF measured values are given. Small error bars are contained within the symbol. (For interpretation of the references to color in this figure legend, the reader is referred to the Web version of this article.)

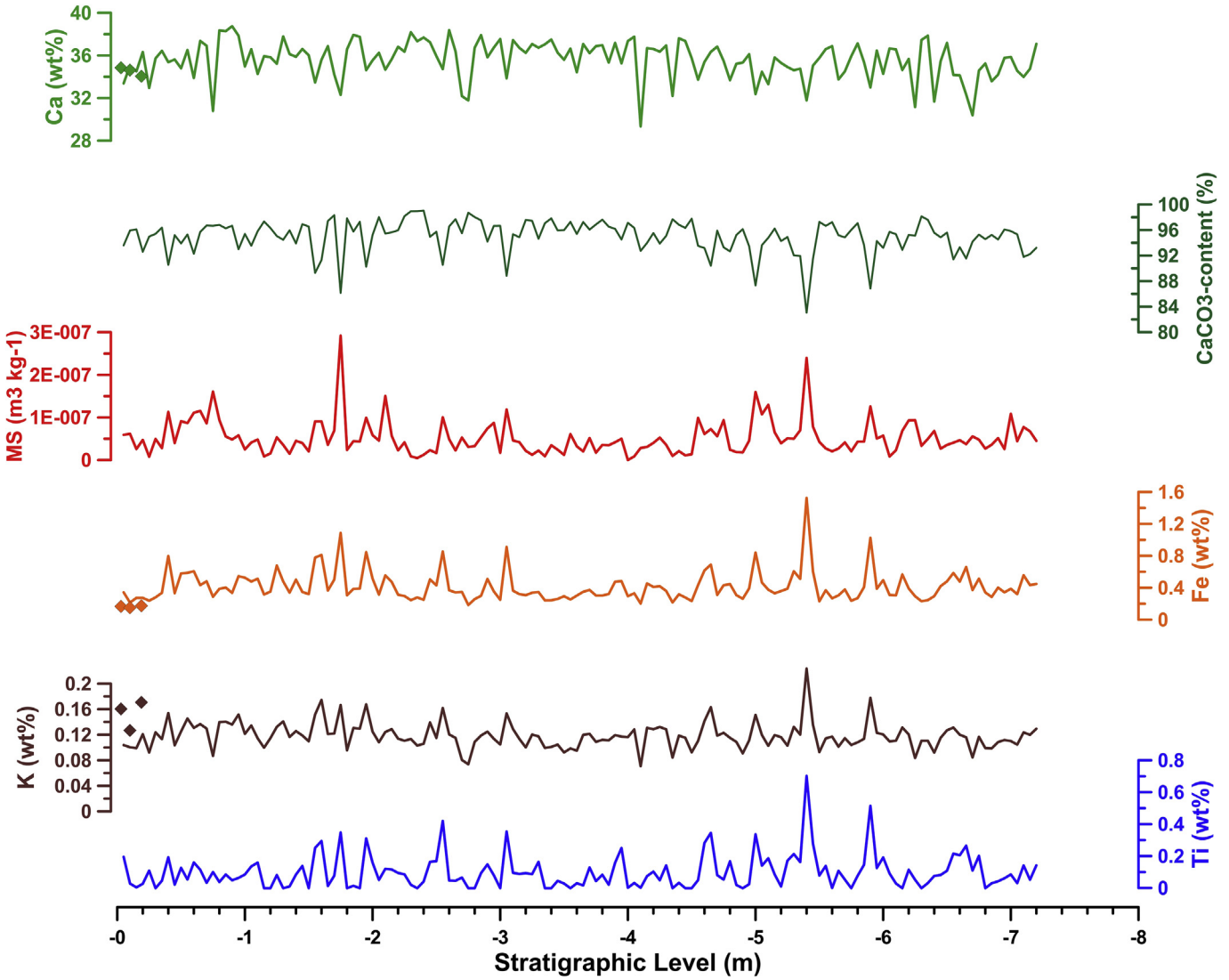

Fig. 4. Multi-proxy record containing new pXRF elemental data and well established magnetic susceptibility and calcium carbonate content records measured by Sinnesael et al. (2016a). Elemental data (Ti-blue, K-brown, Fe-orange, Ca-green) are measured on the powdered samples with the pXRF. ICP-MS bulk data from the same stratigraphic interval as measured by Sosa-Montes de Oca et al. (2017) are indicated with diamond symbols between 0 and −0.2 m. (For interpretation of the references to color in this figure legend, the reader is referred to the Web version of this article.)

To evaluate the potential for cyclostratigraphic analyses, we carried out sliding window (window size = 2.5 m) fast Fourier transformations (FFT) in Matlab® on records of the classical proxies of MS and calcium carbonate content and pXRF measurements of Fe, Ca, Ti and K concentrations along the 7.2 m long section. The algorithms were modified from Muller and MacDonald (2000) and are explained in detail by Bice et al. (2012). The data were linearly detrended and padded with zeros prior to analysis.

4. Results

The calibration for the Sr concentrations based on the reference materials measured by pXRF in this study shows the highest Pearson's r coefficient ($\rho = 1.00$) and a slope close to one (0.94) (Table 1; Fig. 3). The only Sr concentration that does not fall within one standard deviation (1σ) error of the regression is that of the COQ-1 standard, which also has the highest Sr concentration (Tab. S1 Carbonate Reference Materials). High Pearson's r coefficients ($\rho > 0.99$) are also found for the concentration calibration curves for Ca, Mn and Fe, for which all measured values of the elemental concentrations of the reference materials fall within 1 σ errors (Table 1). A lower Pearson's r coefficient ($\rho = 0.95$) is found for the calibration curve of Ti concentrations, because only five reference materials had certified values for Ti concentrations and for only 4 of these reference materials the pXRF measurements are above the detection limit. The less good calibration curve for the Ti concentrations is also evident from the large relative error on the slope for Ti, which is higher than those of the Ca, Mn, Fe and Sr calibrations (Table 1). The correlation for the K concentration calibration is the weakest with a Pearson's r coefficient of 0.54 in combination with a large error on the slope (0.17 ± 9.04).

The pattern of the elemental concentrations profiles of K, Fe and Ti shows the same pattern of the MS signal (Fig. 4). Pearson's r coefficients of 0.56, 0.72 and 0.63 are found for linear regressions between K, Fe and Ti on the one hand against MS on the other hand. Both records are characterized by two intervals of high variation (around −2 and −5.5 m relative to the K-Pg boundary) and intervals with less variation around −1, −4 and −7 m. Although the corre-

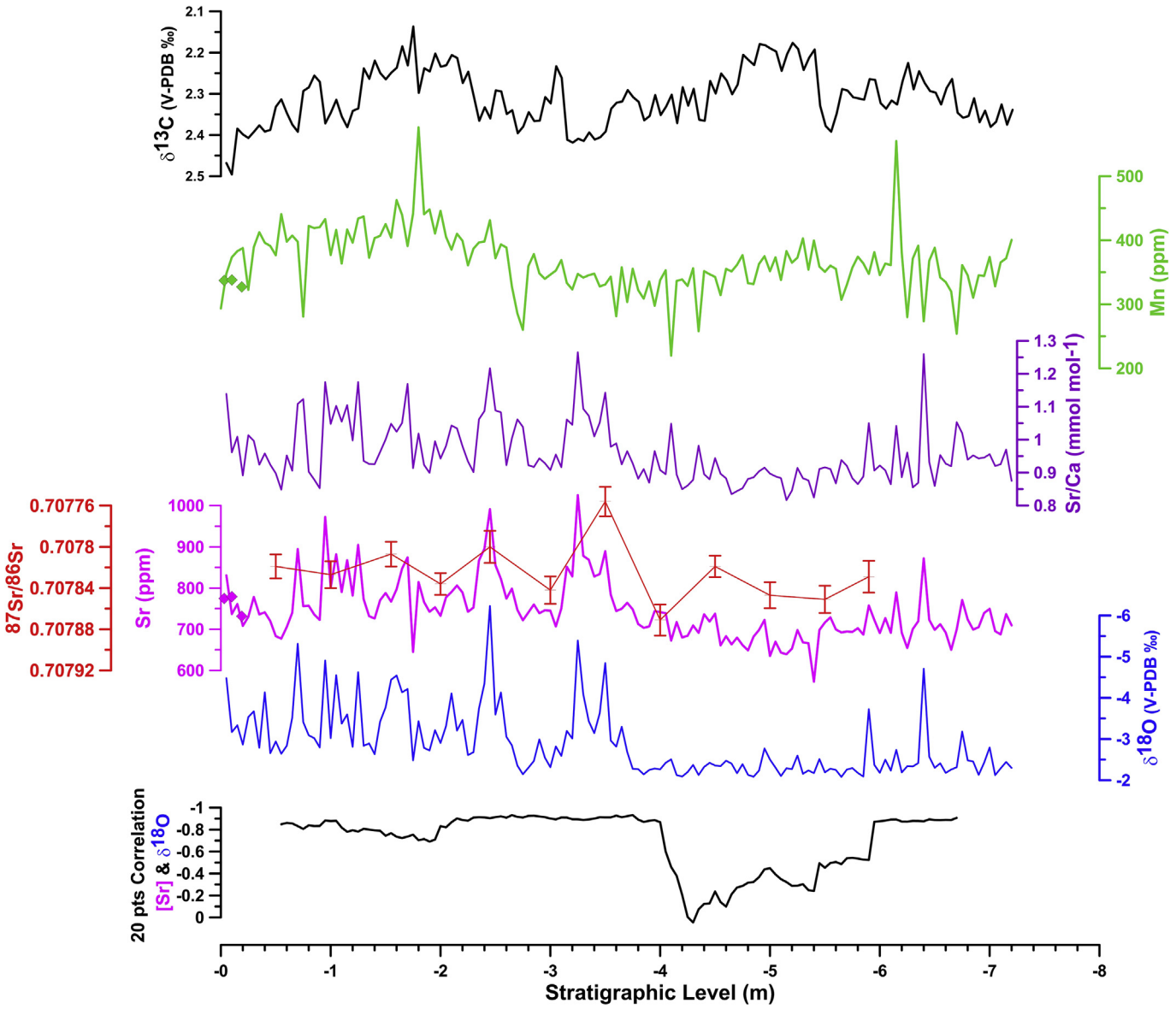

Fig. 5. 20-point running correlation between bulk $\delta^{18}O$ (blue line, inverted axis) and calibrated Sr concentrations (pink line). Sr-isotope ($^{87}Sr/^{86}Sr$) data are indicated in red, the axis is inverted. Mn (green) and Sr (magenta) concentrations are shown, as well as Sr/Ca ratios (thin purple line) and bulk $\delta^{13}C$ ratios (black). The concentrations for Sr and Mn are calibrated and compared with ICP-MS bulk data from the same stratigraphic interval as measured by Sosa-Montes de Oca et al. (2017) (diamond symbols between 0 and −0.2 m). (For interpretation of the references to color in this figure legend, the reader is referred to the Web version of this article.)

lation for the K concentration calibration is much weaker than for Fe and Ti, their relative variations remain similar. The calcium carbonate content also shows increased variation around −2 and −5.5 m, and intervals with less variation around −1, −4 and −7 m (Fig. 4). Minima in calcium carbonate content correspond with maxima in MS, K, Fe and Ti. The Pearson's r coefficient between MS and calcium carbonate content (−0.66) is closer to −1 than the Pearson's r coefficient between calcium carbonate content and the pXRF Ca record is (−0.30). The Mn concentration record displays two maxima around −2 and −5.5 m and a minimum around −1, −4 and −7 m, which is similar – though slightly shifted downwards stratigraphically– to the $\delta^{13}C$ signal (Fig. 5). While the variation in Sr concentrations is rather limited in the lower part of the record (between −4 and −7.2 m), the upper part (between 0 and −4 m) is characterized by peaks of up to 200 ppm relative to the baseline values around 700–800 ppm (Fig. 5). The variation in the Sr record shows an antiphase correlation with the $\delta^{18}O$ signal (Pearson's r coefficient = −0.85), i.e. levels with enrichments in Sr correspond to lower bulk $\delta^{18}O$ values; which is illustrated by running correlation coefficient as plotted in Fig. 5.

Results for the $^{87}Sr/^{86}Sr$ analyses vary between 0.70788 and 0.70776 with a baseline value around 0.70785 (Fig. 5). These values fall within the range of those previously published for the upper Maastrichtian from various sections worldwide (e.g. Sugarman et al., 1995; Vonhof and Smit, 1997; McArthur et al., 1998; Bralower et al., 2004). The two lowest values (at −3.50 and −2.45 m) correspond to levels with enrichments in Sr concentration and pronounced negative $\delta^{18}O$ values (Fig. 5 with an inverted y-axis for the $^{87}Sr/^{86}Sr$ values).

The μXRF mapping and line scanning of the polished hand sample (BOT, −1.50 m) show enrichments in the calcite veins (relative to the surrounding pink matrix) of Ca and Sr concentrations (Fig. 6). The μXRF Sr concentration map shows that the large calcite vein is relatively more enriched in Sr than the smaller veins.

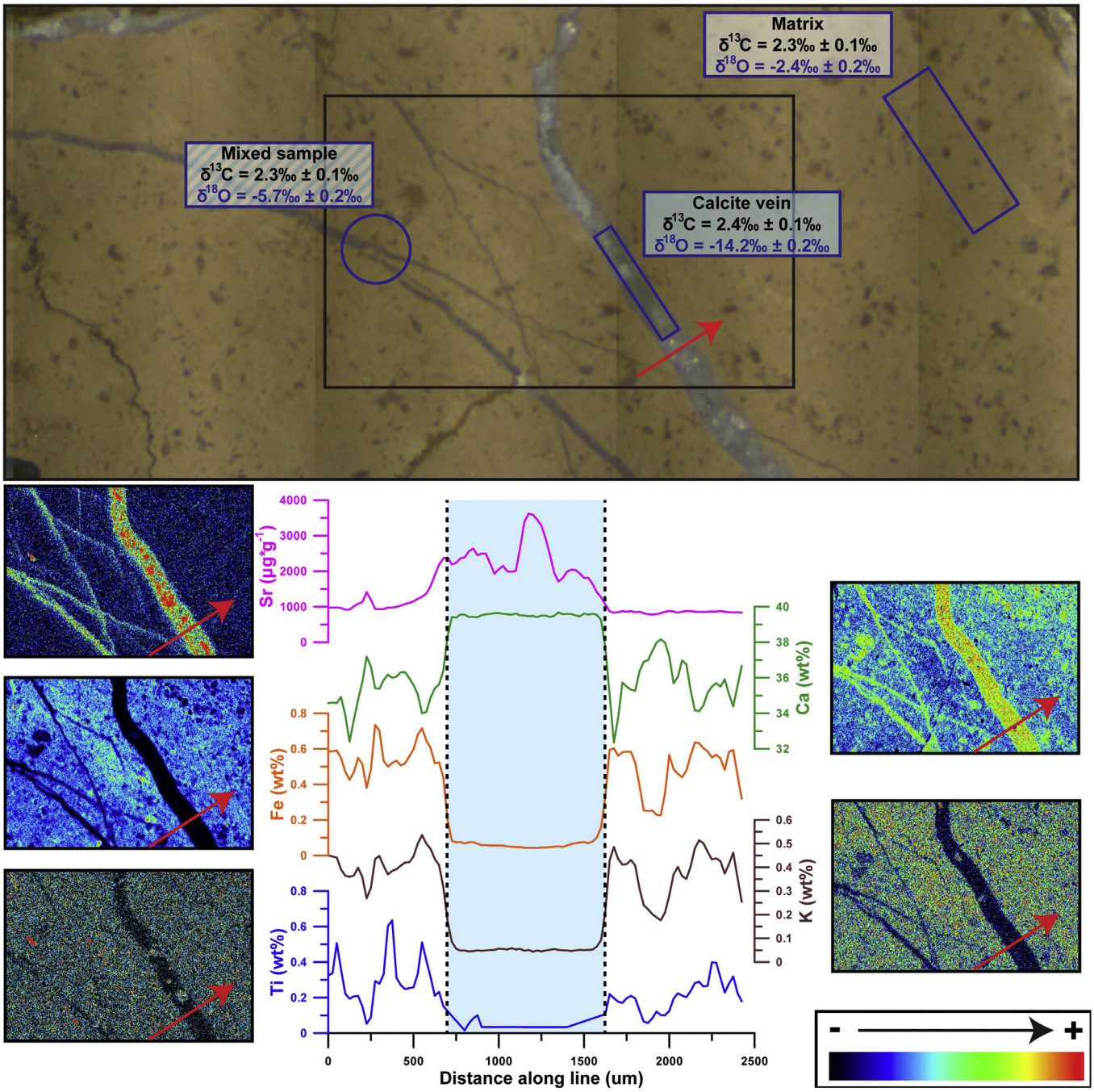

Fig. 6. A polished hand sample containing a clear calcite vein taken around level −1.50 m in the BOT section and analyzed for stable isotope and trace element signature. The calcite veins show lower $\delta^{18}O$ values and unaltered $\delta^{13}C$ values compared to the matrix. The calcite veins are also enriched in Ca and Sr, and depleted in Fe, K and Ti.

The Sr concentration line scan over the large calcite vein shows a doubling to tripling of the Sr concentrations compared to the surrounding pink matrix. All calcite veins are depleted in concentrations of Fe, K and Ti. The $\delta^{18}O$ value of the drilled pink matrix (−2.4‰) is close to the maximum values of the general bulk $\delta^{18}O$ record in the same interval (Figs. 2 & 6). The $\delta^{18}O$ of the pure calcite coming from the calcite vein is about 12‰ lower (−14.2‰), while the sample with mixed calcite vein and surrounding pink matrix has a $\delta^{18}O$ signature (−5.7‰) that resembles the minimum values found in the bulk $\delta^{18}O$ record. The $\delta^{13}C$ values for all tree samples are undistinguishable within the error (2.3 ± 0.1‰) and correspond with the bulk $\delta^{13}C$ record in the same interval (Figs. 2 & 6).

5. Discussion

5.1. Portable XRF calibration

To evaluate the pXRF calibration, we compared our calibrated elemental concentrations with the results obtained on the same section by neutron activation, ICP-MS and ICP-OES by Renard et al. (1982), Smit and Ten Kate (1982), and Sosa-Montes de Oca et al. (2017; Table 2). For this comparison, we looked at the range of values for the bulk measurements carried out in the uppermost 20 cm of the BOT Maastrichtian (Table 2). Comparisons at specific stratigraphic levels with the recent Sosa-Montes de Oca et al. (2017)

Table 2
Comparison of the elemental concentrations of K, Ca, Mn, Fe and Sr between different studies for the uppermost (20 cm) Maastrichtian strata of the BOT section.

	K (ppm)	Ca (wt.%)	Mn (ppm)	Fe (ppm)	Sr (ppm)
This study	991–1038	33–35	348–383	2100–3300	737–830
Sosa-Montes de Oca et al. (2017)	1300–1700	34–35	327–338	1486–1748	731–773
Smit and Ten Kate (1982)	2175 ± 371	38.6 ± 2.6	//	2400 ± 800	706 ± 166
Renard et al. (1982)	//	//	//	//	700–800

data are indicated by diamond symbols on Figs. 4 and 5 (Mn and Sr concentrations from personal communication Claudia Sosa-Montes de Oca). The K concentrations are substantially different than those in the other studies (Table 2), which could be related to high uncertainties in the calibration for the K (see Table 1) and/or the high detection limit for K of the pXRF. The acquired absolute concentrations of Ca, Mn, Fe and Sr from this study overlap with previous independent studies, except for the Fe concentrations compared to Sosa-Montes de Oca et al. (2017; Table 2). The other studies did not provide any results for Ti, which hampers comparison for this element. A commonly used alternative XRF method is core scanning. For example, Giorgioni et al. (2017) used a XRF core scanner on the Piobbico core from the Marne a Fucoidi Formation (consisting mainly of pelagic marlstone, marly limestones, interbedded with black shales) of the Umbria-Marche Basin and reported statistically confident results for Al, Si, K, Ca, Ti, Cr, Mn, Fe and Ba. Reliable Al and Ba measurement are possible with the core scanner because of its higher excitation energy compare to the pXRF. Si was not quantified properly with this pXRF setup because the (soil) fundamental parameter quantification of the pXRF uses SiO_2 mass fraction to sum the total weight to 100%. Cr was measured with the pXRF but the used reference materials did not include certified values for Cr not allowing for a proper calibration to absolute concentrations. Overall, in comparison with afore mentioned studies, the calibration of pXRF results to absolute concentrations appears to yield good results for Ca, Mn, Fe and Sr ($\rho > 0.99$, Table 1), while different pXRF setups or other methods like ICP-MS and XRF core scanning could provide reliable results for other elements (e.g. Al, Si, Ti, Cr, Ba).

5.2. Detrital proxies and cyclostratigraphy

The studied sediments consist primarily of biogenic calcite (foraminifera and coccoliths) with a fine fraction (clay to silt) most likely consisting of windblown dust (Arthur and Fischer, 1977; Johnsson and Reynols, 1986; Savain et al., 2014). Based on the study of magnetic properties, Savain et al. (2014) proposed eolian dust deposition for the Eocene sediments of the Umbria-Marche basin. Calderoni and Ferrini (1984) also showed that the K-feldspars and Fe-content of the Scaglia Rossa sediments are associated with the residual (i.e. non-carbonate, non-soluble) fraction. The detrital elements (K, Ti, Fe) and MS all show a similar pattern and track the presence of the eolian dust component. This pattern is opposite to that of Ca, which reflects the amount of biogenic calcium carbonate. Sinnesael et al. (2016a) proposed that the availability of windblown dust, and thus higher level of detrital elements, is a function of monsoon dominated precipitation patterns over the North African continent, and hypothesized an orbital forcing influence because of the relationship between the monsoon and the precessional configuration. Provenance analysis of detrital zircons from the lowermost Danian in the BOT section also suggests a North-African source for dust supply (Aguirre-Palafox et al., 2017). In this interpretation, the detrital elements (K, Ti and Fe) can be interpreted in a paleoclimatological way and these proxy records constitute good candidates for cyclostratigraphic analyses.

The main pattern of frequency-power distribution over the record as shown on the evolutionary FFT's is robust for most elements (Fig. 7). This main pattern, for all elements except Ca, consists of a dominant periodicity around 2 cycles m^{-1} in the lower half of the stratigraphic interval (Fig. 7). Sinnesael et al. (2016a) interpreted this 2 cycles m^{-1} cycle as the result of forcing by the obliquity cycle. The power of this frequency band with 2 cycles m^{-1} generally gets weaker in the upper part of the section (between 0 and −3.5 m), whereas in the same interval the power around frequencies around 1 and 5–6 cycles m^{-1} get higher. The first one is related to short eccentricity, while the latter one corresponds to the precession band (Sinnesael et al., 2016a). There are subtle differences between the results of the different proxies. For example, the obliquity-associated component for the MS signal is concentrated with a high power around 2 cycles m^{-1} (Fig. 7). However, the same power is present in two weaker peaks at slightly lower and higher frequencies for K, Ti, Fe and the $CaCO_3$ (Fig. 7). This can probably be explained by the fact that FFT analyses do not have a unique solution for frequency and amplitude; as such (small) variations in the analyzed input signals can result in slightly different decomposition into frequency and amplitude. Another dissimilarity is the apparent continuity of the precession-associated component for the potassium proxy over the whole record, instead of only for the upper part of for example MS and Fe (Fig. 7). It could be explained by K having the worst calibration of all investigated elements (Table 1 and Fig. 3). However, despite the offset in absolute values, the relative variation in the K concentration signal can still be used for cyclostratigraphic analyses. As such, for cyclostratigraphic applications which mainly look at relative variations, one could work with uncalibrated results for K or other elements (e.g. the net counts of the spectrum). A more pronounced difference in the moving window FFT pattern can be observed in the Ca than in the detrital elements, where a 4–5 cycles m^{-1} dominates the spectrum (Fig. 7). In contrast with K, the calibration for the Ca concentrations with the pXRF measurements calibration is reliable (Table 1 and Fig. 3). Potentially, the relative smaller difference in relative variations in the Ca signal compared to for example the MS signal could cause this discrepancy (Fig. 4).

In general, results of the cyclostratigraphical analysis are similar for most investigated proxies and the actual resemblances and differences between them enable the evaluation of the robustness of signals and the validity of their interpretations. The Fe concentrations show the highest correlation with MS, and yield the most reliable results in pXRF measurements (ideal in spectrum range, detectable concentrations), therefore, we advocate that pXRF measured Fe concentrations constitute a suitable alternative for the classical MS measurements for cyclostratigraphic analyses in pelagic carbonate settings, such as the one described in this study. The aim of this study is not to replace classical MS or calcium carbonate content measurements, but to investigate the advantages of using pXRF, as an alternative compared to the conventional methods. The asset of the pXRF approach is that concentrations of several elements can be acquired at once, the measurements are non-destructive and measurement time is relatively short, allowing for increased sample throughput in comparison with conventional methods.

5.3. Chemostratigraphical applications

Carbon stable isotopes ($\delta^{13}C$), Sr/Ca ratios, Sr and Mn concentrations in carbonates are often used for chemostratigraphical applications. The $\delta^{13}C$ record measured by Sinnesael et al. (2016a) corresponds well with the BOT $\delta^{13}C$ record measured by Voigt

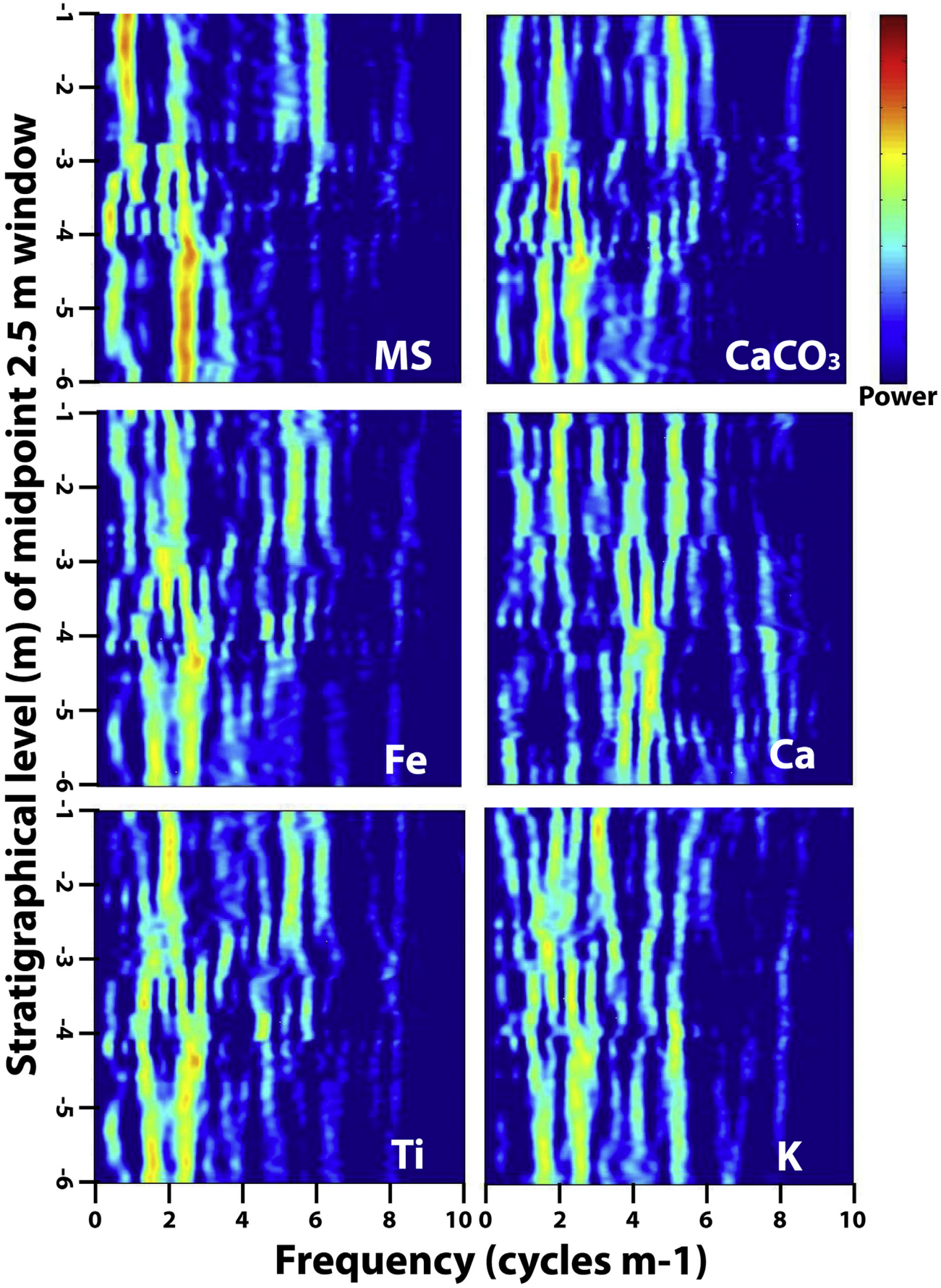

Fig. 7. Moving window (2.5 m) fast Fourier Transforms of the magnetic susceptibility (MS), calcium carbonate content ($CaCO_3$), Fe, Ca, Ti and K.

et al. (2012) who incorporated it in a global correlation for the upper Campanian to Maastrichtian. The test of sampling both calcite veins and micritic matrix showed that the $\delta^{13}C$ results are not affected by the sampling of the calcite veins (Fig. 6). The upper Maastrichtian $\delta^{13}C$ record from BOT was also incorporated in the Late Cretaceous compilation by Wendler (2013), who also provided a comprehensive review on principles of carbon isotope stratigraphy. The μXRF mapping and line scanning demonstrate clearly that peak enrichments in Sr concentrations are caused by sampling calcite veins while drilling for sample powder (Fig. 6). This contamination makes it difficult to interpret the fine-scale variability in the Sr record in a chemostratigraphical context, but the bulk Sr/Ca ratios measured with the pXRF are still in agreement with previously published studies (Fig. 6; Renard, 1986; Stoll and Schrag, 2001; Jarvis et al., 2008). The μXRF mapping, in combination with the stable isotope analysis, also explains the observed covariation between Sr enrichments and negative $\delta^{18}O$ excursions (sampling of the calcite veins) (Fig. 5). Next to variable contributions in $\delta^{18}O$ from the micrite cement, the size of these anomalies is also a function of the proportion (mass balance) of sampled and measured matrix versus calcite vein. This can be an explanation for the proposed diagenetic imprint on whole rock stable isotope analyses in the Bottaccione Gorge by Corfield et al. (1991) and suggest a more careful interpretation of the bulk $\delta^{18}O$ record of Sinnesael et al. (2016a). This illustrates again how cautious one has to be while sampling for bulk rock stable isotope analysis. Instead of drilling the powder straight from the rock, we propose to continue with common practice and take hand samples first and then (micro-) drill the fine micrite prior to isotopic and trace elemental analyses. The bulk $^{87}Sr/^{86}Sr$ seem to be little affected by these Sr enrichments, except for potentially two samples (BOT, −2.45 m and −3.50 m) with slightly lower $^{87}Sr/^{86}Sr$ values, although these almost overlap within the error (2 σ). Some studies also use Mn contents in carbonates as chemostratigraphical tool, with hydrothermal activity being the dominant source of Mn in seawater (e.g. Jarvis et al., 2001, 2008; La Callonec et al., 2014). In general, chemostratigraphical interpretations of Sr (Sr/Ca ratios) and Mn concentrations can be an additional benefit in a multi-proxy approach facilitated by the pXRF.

6. Conclusions

This study presents an integrated multi-proxy dataset with calibrated pXRF data and interpretations for a selection of elements (K, Ca, Ti, Mn, Fe, Sr) from the uppermost Maastrichtian pelagic carbonates of the Bottaccione Gorge, Gubbio, Italy. The applied multi-standard calibration based on pXRF measurements of powdered reference materials yields calibrated results of elemental concentrations, with varying reliability (Pearson's calibration regression coefficients > 0.99 for Ca, Mn, Fe, and Sr), which are comparable with independent ICP-MS and atomic absorption spectroscopy results from the same strata. The detrital pXRF elemental data (K, Fe, and Ti) confirm the hypothesis that magnetic susceptibility in these pelagic carbonates constitutes a good proxy for detrital input. Especially the Fe-content corresponds well with the magnetic susceptibility. The detrital component (e.g. Fe) of pelagic carbonates traces climatic variations that influenced the source and amount of detrital material transported into the basin. As such, the suitability of detrital pXRF elemental data for cyclostratigraphy is demonstrated. Although pXRF measurements of Ca approximate the calcium carbonate content, the signal appears less suitable for cyclostratigraphic analysis than Fe concentrations, for example. Other elemental pXRF data such as Mn and Sr can be used (on a local or regional scale), together with the conventional $\delta^{13}C$ proxy (more global scale) for chemostratigraphy. Moreover, we demonstrate enrichments in Sr concentrations and lower $\delta^{18}O$ values due to a calcite vein sampling bias (next to other potential variations in micrite cement) in some our samples on the bulk $\delta^{18}O$ signal and Sr-concentrations. However, the $\delta^{13}C$ and Sr-isotope signals of the uppermost Maastrichtian in the Bottaccione Gorge, Gubbio, Italy, seem little affected by this sampling effect. Overall, with proper measurement strategies and careful calibration, pXRF measurements can be an additional, reliable, relatively easy, non-destructive, less expensive, and relatively fast method to acquire multi-elemental concentration data from pelagic carbonates, with numerous application in paleo-environmental studies and cyclostratigraphy.

Acknowledgments

We thank Claudia Sosa-Montes de Oca for sharing the Mn (ICP-OES) and Sr (ICP-MS) data. This research is supported by the Association “Le Montagne di San Francesco” in Coldigioco, Italy. Matthias Sinnesael thanks the Research Foundation of Flanders (FWO) for the awarded PhD Fellowship (FWOTM782) and Niels J. de Winter thanks IWT for the awarded PhD Flanders Fellowship (IWT700-SB-141047). Dr. C. Snoeck is supported by Research Foundation of Flanders (FWO) post-doctoral fellowship. Philippe Claeys thanks the FWO-Hercules foundation for financing the XRF analytical platform at the VUB, and the VUB strategic research funding. We thank the handling editor, Eduardo Koutsoukos, Nicolas Thibault and an anonymous reviewer for constructive comments which helped to improve this manuscript.

References

Adcock, R.J., 1878. A problem in least squares. The Analyst 5, 53–54. https://doi.org/10.2307/2635758.

Aguirre-Palafox, L.E., Alvarez, W., Schmitz, B., 2017. U-Pb ages of detrital zircons from pelagic limestones: Apennine samples and provenance analysis. Geological Society of America with Programs 49 (6). https://doi.org/10.1130/abs/2017AM-306429.

Alvarez, L.W., Alvarez, W., Asaro, F., Michel, H.V., 1980. Extraterrestrial cause for the Cretaceous-Tertiary extinction. Science 208, no. 4448, 1095–1108. https://doi.org/10.1126/science.208.4448.1095.

Arthur, M.A., Fischer, A.G., 1977. Upper Cretaceous–Paleocene magnetic stratigraphy at Gubbio, Italy I. Lithostratigraphy and sedimentology. Geological Society of America Bulletin 88 367. https://doi.org/10.1130/0016-7606(1977)88<367:UCMSAG>2.0.CO;2.

Batenburg, S.J., De Vleeschouwer, D., Sprovieri, M., Hilgen, F.J., Gale, A.S., Singer, B.S., Koeberl, C., Coccioni, R., Claeys, P., Montanari, A., 2016. Orbital control on the timing of oceanic anoxia in the Late Cretaceous. Climate of the Past 12, 1995–2009. https://doi.org/10.5194/cp-12-1995-2016.

Bice, D., Montanari, A., Vučetić, V., Vučetić, M., 2012. The influence of regional and global climatic oscillations on Croatian climate. International Journal of Climatology 32, 1537–1557. https://doi.org/10.1002/joc.2372.

Bralower, T.J., Fullagar, P.D., McCay, T.A., MacLeod, K.G., Bergen, J., Zapata, E., 2004. Strontium isotope stratigraphy of Cretaceous sediments at Sites 1183 and 1186, Ontong Java Plateau. In: Proceedings of the Ocean Drilling Program, Scientific Results. https://doi.org/10.2973/odp.proc.sr.192.106.2004.

Calderoni, G., Ferrini, V., 1984. Abundances and chemical fractionation of Al, Fe, Mn, Zn, Pb, Cu and Tl in Cretaceous-Palaeocene limestones from Gubbio (Central Italy). Geochemical Journal 18, 31–41. https://doi.org/10.2343/geochemj.18.31.

Cleaveland, L.C., Jensen, J., Goese, S., Bice, D.M., Montanari, A., 2002. Cyclostratigraphic analysis of pelagic carbonates at Monte dei Corvi (Ancona, Italy) and astronomical correlation of the Serravallian-Tortonian boundary. Geology 30, 931–934. https://doi.org/10.1130/0091-7613(2002)030<0931:CAOPCA>2.0.CO;2.

Coccioni, R., Premoli Silva, I., 2015. Revised upper Albian–Maastrichtian calcareous plankton biostratigraphy and magneto-stratigraphy of the classical Tethyan Gubbio section (Italy). Newsletters on Stratigraphy v. 48, 47–90. https://doi.org/10.1127/nos/2015/0055.

Corfield, R.M., Cartlidge, J.E., Premoli-Silva, I., Housley, R.A., 1991. Oxygen and carbon isotope stratigraphy of the Palaeogene and Cretaceous limestones in the Bottaccione Gorge and the Contessa Highway sections, Umbria, Italy. Terra Nova 3, 414–422. https://doi.org/10.1111/j.1365-3121.1991.tb00171.x.

de Winter, N.J., Sinnesael, M., Makarona, C., Vansteenberge, S., Claeys, P., 2017a. Trace element analyses of carbonates using portable and micro-X-ray fluorescence: Performance and optimization of measurement parameters and strategies. Journal of Analytical Atomic Spectrometry. https://doi.org/10.1039/C6JA00361C.

de Winter, N.J., Goderis, S., Dehairs, F., Jagt, J.W.M., Fraaije, R.H.B., Van Malderen, S.J.M., Vanhaecke, F., Claeys, P., 2017b. Tropical seasonality in the late Campanian (late Cretaceous): Comparison between multiproxy records from three bivalve taxa from Oman, Palaeogeography, Palaeoclimatology. Palaeoecology 485, 740–760. https://doi.org/10.1016/j.palaeo.2017.07.031.

Deming, W.E., 1943. Statistical Adjustment of Data. Dover Publications, Mineola, NY USA, 288 pp.

Galeotti, S., Moretti, M., Cappelli, C., Phillips, J., Lanci, L., Littler, K., Monechi, S., Petrizzo, M.R., Silva, I.P., Zachos, J.C., 2015. The Bottaccione section at Gubbio, central Italy: a classical Paleocene Tethyan setting revisited. Newsletters on Stratigraphy 48, 325–339. https://doi.org/10.1127/nos/2015/0067.

Gardin, S., Galbrun, B., Thibault, N., Coccioni, R., Premoli Silva, I., 2012. Bio-magnetostratigraphy for the upper Campanian – Maastrichtian from the Gubbio area, Italy: new results from the Contessa Highway and Bottaccione sections. Newsletters on Stratigraphy 45, 75–103. https://doi.org/10.1127/0078-0421/2012/0014.

Giorgioni, M., Tiraboschi, D., Erba, E., Hamann, Y., Weissert, H., 2017. Sedimentary patterns and palaeoceanography of the Albian Marne a Fucoidi Formation (Central Italy) revealed by high-resolution geochemical and nannofossil data. Sedimentology 64, 111–126. https://doi.org/10.1111/sed.12288.

Herbert, T.D., Stallard, R.F., Fischer, A.G., 1986. Anoxic events, productivity rhythms, and the orbital signature in a Mid-Cretaceous deep-sea sequence from central Italy. Paleoceanography 1, 495–506. https://doi.org/10.1029/PA001i004p00495.

Husson, D., Galbrun, B., Gardin, S., Thibault, N., 2014. Tempo and duration of short-term environmental perturbations across the Cretaceous-Paleogene boundary. Stratigraphy 11, 159–171.

Husson, D., Galbrun, B., Thibault, N., Gardin, S., Huret, E., Coccioni, R., 2012. Astronomical duration of polarity Chron C31r (Lower Maastrichtian): cyclostratigraphy of ODP Site 762 (Indian Ocean) and the Contessa Highway section (Gubbio, Italy). Geological Magazine 149, 345–351. https://doi.org/10.1017/S0016756811000999.

Ibáñez-Insa, J., Pérez-Cano, J., Fondevilla, V., Oms, O., Rejas, M., Fernández-Turiel, J.L., Anadón, P., 2017. Portable X-ray fluorescence identification of the Cretaceous–Paleogene boundary: Application to the Agost and Caravaca sections, SE Spain. Cretaceous Research 78, 139–148. https://doi.org/10.1016/j.cretres.2017.06.004.

Jarvis, I., Murphy, A.M., Gale, A.S., 2001. Geochemistry of pelagic and hemipelagic carbonates: criteria for identifying systems tracts and sea-level change. Journal of the Geological Society 158, 685–696. https://doi.org/10.1144/jgs.158.4.685.

Jarvis, I., Mabrouk, A., Moody, R.T.J., Murphy, A.M., Sandman, R.A., 2008. Applications of carbon isotope and elemental (Sr/Ca, Mn) chemostratigraphy to sequence analysis: sea-level change and the global correlation of pelagic carbonates. In: Salem, M.J., El-Hawat, A.S. (Eds.), The Geology of East Libya, vol. 1. Earth Science Society of Libya, Tripoli, Libya, pp. 369–396.

Johnsson, M.J., Reynols, R.C., 1986. Clay mineralogy of shale-limestone rhythmites in the Scaglia rossa (Turonian-Eocene), Italian Apennines. Journal of Sedimentary Research 56, 501–509. https://doi.org/10.1306/212F896D-2B24-11D7-8648000102C1865D.

Kummell, C.H., 1879. Reduction of observation equations which contain more than one observed quantity. The Analyst 97–105. https://doi.org/10.2307/2635646.

Le Callonec, L., Renard, M., De Rafélis, M., Minoletti, F., Beltran, C., Du Chêne, R.J., 2014. Evolution of trace element contents (Sr and Mn) of hemipelagic carbonates from the Zumaia Paleocene section (Gipuzkoa, Spain): implications for the knowledge of seawater chemistry during the Selandian. Bulletin de la Société Géologique de France 185, 413–435. https://doi.org/10.2113/gssgfbull.185.6.413.

Lowrie, W., Alvarez, W., Asaro, F., 1990. The origin of the white beds below the Cretaceous-Tertiary boundary in the Gubbio section, Italy. Earth and Planetary Science Letters 98, 303–312. https://doi.org/10.1016/0012-821X(90)90032-S.

Lowrie, W., Alvarez, W., Napoleone, G., Perch-Nielsen, K., Silva, I.P., Toumarkine, M., 1982. Paleogene magnetic stratigraphy in Umbrian pelagic carbonate rocks: The Contessa sections, Gubbio. Geological Society of America Bulletin 93 414. https://doi.org/10.1130/0016-7606(1982)93<414:PMSIUP>2.0.CO;2.

Luterbacher, H.P., Premoli Silva, I., 1964. Biostratigrafi a del limite creteceo-terziario nell'Appennino central. Rivista Italiana di Paleontologia e Stratigrafia 70, 67–128.

McArthur, J.M., Thirwall, M.F., Engkildec, M., Zinsmeisterd, W.J., Howartha, R.J., 1998. Strontium isotope profiles across K/T boundary sequences in Denmark and Antarctica. Earth and Planetary Science Letters 160, 179–192. https://doi.org/10.1016/S0012-821X(98)00058-2.

Montanari, A., Chan, L.S., Alvarez, W., 1989. Synsedimentary tectonics in the Late Cretaceous–early Tertiary pelagic basin of the Northern Apennines. In: Crevello, P., Wilson, J.L., Sarg, R., Reed, F. (Eds.), Controls on Carbonate Platforms and Basin Development: Society of Economic Paleontologists and Mineralogists Special Publication, 44, pp. 379–399. https://doi.org/10.2110/pec.89.44.0379.

Montanari, A., Farley, K., Claeys, P., De Vleeschouwer, D., de Winter, N., Vansteenberge, S., Sinnesael, M., Koeberl, C., 2017. Stratigraphic record of the asteroidal Veritas breakup in the Tortonian Monte dei Corvi section (Ancona, Italy). The Geological Society of America Bulletin 129, 1357–1376. https://doi.org/10.1130/B31476.1.

Mukhopadhyay, S., 2001. A short duration of the Cretaceous-Tertiary boundary event: evidence from extraterrestrial helium-3. Science 291, 1952–1955. https://doi.org/10.1126/science.291.5510.1952.

Muller, R.A., MacDonald, G.J., 2000. Ice Ages and Astronomical Causes. Data, Spectral Analysis and Mechanisms. Springer, London, 318 pp.

Potts, P.J., Bernardini, F., Jones, M.C., Williams-Thorpe, O., Webb, P.C., 2006. Effects of weathering onin situ portable X-ray fluorescence analyses of geological outcrops: dolerite and rhyolite outcrops from the Preseli Mountains, South Wales. X-Ray Spectrometry 35, 8–18. https://doi.org/10.1002/xrs.881.

Quye-Sawyer, J., Vandeginste, V., Johnston, K.J., 2015. Application of handheld energy-dispersive X-ray fluorescence spectrometry to carbonate studies: opportunities and challenges. Journal of Analytical Atomic Spectrometry 30, 1490–1499. https://doi.org/10.1039/C5JA00114E.

R Development Core Team, 2008. R: A Language and Environment for Statistical Computing. R Foundation for Statistical Computing, Vienna, Austria. ISBN 3-900051-07-0, URL. http://www.R-project.org.

Renard, M., 1986. Pelagic carbonate chemostratigraphy (Sr, Mg, 18O, 13C). Marine Micropaleontology 10, 117–164. https://doi.org/10.1016/0377-8398(86)90027-7.

Renard, M., Delacotte, O., Letolle, R., 1982. Le strontium et les isotopes stables dans les carbonates totaux de quelques sites de l'Atlantique et de la Tethys. Bulletin de la Societe Geologique de France S7-XXIV 519–534. https://doi.org/10.2113/gssgfbull.S7-XXIV.3.519.

Robinson, N., Ravizza, G., Coccioni, R., Peucker-Ehrenbrink, B., Norris, R., 2009. A high-resolution marine 187Os/188Os record for the late Maastrichtian: distinguishing the chemical fingerprints of Deccan volcanism and the KP impact event. Earth and Planetary Science Letters 281, 159–168. https://doi.org/10.1016/j.epsl.2009.02.019.

Savain, J.F., Jovane, L., Frontalini, F., Trindade, R.I.F., Coccioni, R., Bohaty, S.M., Wilson, P.A., Florindo, F., Roberts, A.P., Catanzariti, R., Iacoviello, F., 2014. Enhanced primary productivity and magnetotactic bacterial production in response to middle Eocene warming in the Neo-Tethys Ocean. Palaeogeography, Palaeoclimatology, Palaeoecology 414, 32–45. https://doi.org/10.1016/j.palaeo.2014.08.009.

Sherman, J., 1955. The theoretical derivation of fluorescent X-ray intensities from mixtures. Spectrochimica Acta 7, 283–306. https://doi.org/10.1016/0371-1951(55)80041-0.

Sinnesael, M., De Vleeschouwer, D., Coccioni, R., Claeys, P., Frontalini, F., Jovane, L., Savian, J.F., Montanari, A., 2016a. High-resolution multiproxy cyclostratigraphic analysis of environmental and climatic events across the Cretaceous-Paleogene boundary in the classic pelagic succession of Gubbio (Italy). In: Geological Society of America Special Papers. Geological Society of America, pp. 115–137. https://doi.org/10.1130/2016.2524(09).

Sinnesael, M., Zivanovic, M., De Vleeschouwer, D., Claeys, P., Schoukens, J., 2016b. Astronomical component estimation (ACE v.1) by time-variant sinusoidal modeling. Geoscientific Model Development 9, 3517–3531. https://doi.org/10.5194/gmd-9-3517-2016.

Smit, J., Ten Kate, W., 1982. Trace-element patterns at the Cretaceous-Tertiary boundary—consequences of a large impact. Cretaceous Research 3, 307–332. https://doi.org/10.1016/0195-6671(82)90031-3.

Snoeck, C., Lee-Thorp, J., Schulting, R., de Jong, J., Debouge, W., Mattielli, N., 2015. Calcined bone provides a reliable substrate for strontium isotope ratios as shown by an enrichment experiment: Strontium isotope ratios in calcined bone. Rapid Communications in Mass Spectrometry 29, 107–114. https://doi.org/10.1002/rcm.7078.

Sosa-Montes de Oca, C., Rodríguez-Tovar, F.J., Martínez-Ruiz, F., Monaco, P., 2017. Paleoenvironmental conditions across the Cretaceous–Paleogene transition at the Apennines sections (Italy): an integrated geochemical and ichnological approach. Cretaceous Research 71, 1–13. https://doi.org/10.1016/j.cretres.2016.11.005.

Stoll, H.M., Schrag, D.P., 2001. Sr/Ca variations in Cretaceous carbonates: relation to productivity and sea level changes. Palaeogeography, Palaeoclimatology, Palaeoecology 168, 311–336. https://doi.org/10.1016/S0031-0182(01)00205-X.

Sugarman, P.J., Miller, K.G., Bukry, D., Feigenson, M.D., 1995. Uppermost Campanian–Maestrichtian strontium isotopic, biostratigraphic, and sequence stratigraphic framework of the New Jersey Coastal Plain. The Geological Society of America Bulletin 107, 19–37. https://doi.org/10.1130/0016-7606(1995)107<0019:UCMSIB>2.3.CO;2.

Thiel, H., 1950. A rank-invariant method of linear and polynomial regression analysis, Part 3. In: Proceedings of Koninklijke Nederlandse Akademie van Wetenschappen A, pp. 1397–1412.

Thibault, N., Ruhl, M., Ullmann, C.V., Korte, C., Kemp, D.B., Gröcke, D.R., Hesselbo, S.P., 2017. The wider context of the Lower Jurassic Toarcian oceanic anoxic event in Yorkshire coastal outcrops, UK. In Press, Corrected Proof Proceedings of the Geologists' Association. https://doi.org/10.1016/j.pgeola.2017.10.007.

Voigt, S., Gale, A.S., Jung, C., Jenkyns, H.C., 2012. Global correlation of Upper Campanian – Maastrichtian successions using carbon-isotope stratigraphy: development of a new Maastrichtian timescale. Newsletters on Stratigraphy 45, 25–53. https://doi.org/10.1127/0078-0421/2012/0016.

Vonhof, H.B., Smit, J., 1997. High-resolution late Maastrichtian–early Danian oceanic 87Sr/86Sr record: Implications for Cretaceous-Tertiary boundary events.

Geology 25, 347–350. https://doi.org/10.1130/0091-7613(1997)025<0347:HRLMED>2.3.CO;2.
Weis, D., Kieffer, B., Maerschalk, C., Barling, J., de Jong, J., Williams, G.A., Hanano, D., Pretorius, W., Mattielli, N., Scoates, J.S., Goolaerts, A., Friedman, R.M., Mahoney, J.B., 2006. High-precision isotopic characterization of USGS reference materials by TIMS and MC-ICP-MS: isotopic study of USGS reference materials. Geochemistry, Geophysics, Geosystems 7. https://doi.org/10.1029/2006GC001283 n/a–n/a.
Wendler, I., 2013. A critical evaluation of carbon isotope stratigraphy and biostratigraphic implications for Late Cretaceous global correlation. Earth-science Reviews 126, 116–146. https://doi.org/10.1016/j.earscirev.2013.08.003.
Young, K.E., Evans, C.A., Hodges, K.V., Bleacher, J.E., Graff, T.G., 2016. A review of the handheld X-ray fluorescence spectrometer as a tool for field geologic investigations on Earth and in planetary surface exploration. Applied Geochemistry 72, 77–87. https://doi.org/10.1016/j.apgeochem.2016.07.003.

Appendix A. Supplementary data

Supplementary data related to this article can be found at https://doi.org/10.1016/j.cretres.2018.04.010.